

Open-air printing of Cu₂O thin films with high hole mobility for semitransparent solar harvesters

Abderrahime Sekkat^{1,2,3}, Viet Huong Nguyen⁴, César Arturo Masse de La Huerta¹, Laetitia Rapenne¹, Daniel Bellet¹, Anne Kaminski-Cachopo², Guy Chichignoud³ & David Muñoz-Rojas¹✉

Cu₂O is a promising p-type semiconductor for low-cost photovoltaics and transparent optoelectronics. However, low-cost and low-temperature fabrication of Cu₂O films with good transport properties remains challenging, thus limiting their widespread adoption in devices. Here, we report Cu₂O thin films of 20–80 nm thickness with hole mobility up to 92 cm²V⁻¹s⁻¹ using atmospheric-pressure spatial atomic layer deposition at temperatures below 260 °C, from a copper (I) hexafluoro-2,4-pentanedionate cyclooctadiene precursor. Raman spectroscopy indicates the presence of copper split vacancies and shows that the high hole mobility can be correlated to a low concentration of shallow acceptor defects. The optical bandgap of deposited films can be tuned between 2.08 eV and 2.5 eV, depending on the deposition temperature. All-oxide semitransparent Cu₂O/ZnO solar harvesters are fabricated, showing efficiency values comparable to devices that incorporate much thicker Cu₂O layers. Our work provides a promising approach towards cost-efficient, all-oxide solar harvesters, and for other (opto)electronic devices.

¹Univ. Grenoble Alpes, CNRS, Grenoble INP, LMGP, Grenoble, France. ²Univ. Grenoble Alpes, Univ. Savoie Mont Blanc, CNRS, Grenoble INP, IMEP-LaHC, Grenoble, France. ³Univ. Grenoble Alpes, CNRS, Grenoble INP, SIMAP, Grenoble, France. ⁴Faculty of Materials Science and Engineering, Phenikaa University, Hanoi, Vietnam. ✉email: david.munoz-rojas@grenoble-inp.fr

C_u₂O is a promising p-type semiconducting oxide that has been extensively studied due to its potential application in many optoelectronic devices. Initial studies involving its photoelectric effect and rectifying behavior date back to the mid-1920s¹, and yielded many fundamental theories in semiconductors. Cu₂O crystallizes in a cuprite structure composed of two sublattices with a direct bandgap of about 1.9–2.1 eV. The need for low-cost solar cells increased the interest in Cu₂O as a potential absorber, given the abundance and nontoxicity of copper, and the potential of Cu-based compounds to provide a better cost-efficiency ratio than the current main technology based on crystalline silicon^{2,3}. Theoretical studies indeed predict a maximum efficiency for single-junction Cu₂O solar cells around 20% under air mass (AM) 1.5 illumination^{4,5}. As a result, copper-based materials have been proposed as potential candidates for new generation solar cells and other energy-related devices^{6–12}.

But one of the greatest challenges when dealing with Cu₂O is to enhance its electrical transport properties, especially when grown by chemical approaches. The native p-type conductivity in Cu₂O is caused by the formation of copper vacancies V_{Cu} that have a shallow energy level and thus act as efficient hole producers¹³. Such V_{Cu} can also be present in the so-called split configuration, $V_{Cu,split}$, which consists of two copper vacancies and a copper interstitial in between the vacancies, both types of copper vacancies having similar formation energies^{14–16}. However, $V_{Cu,split}$ seems to be more stable than normal defects thanks to a better charge balance¹⁴. Indeed, it was demonstrated to be the more favorable defect type, always accompanied by an expected permanent presence of V_{Cu} within the films¹⁶. While Cu vacancies are necessary as hole producers, they can also act as traps during the hole transport process, which eventually limits the hole mobility¹⁷. All these characteristics, combined with the morphological parameters of the material (mainly grain size and mass density), thus play an important role in the resulting transport properties of the films^{18,19}. To date, the reported hole mobility for single-crystal Cu₂O is $\sim 100 \text{ cm}^2 \text{ V}^{-1} \text{ s}^{-1}$ ²⁰. The difficulty in obtaining intrinsic Cu₂O thin films having high hole mobility using low temperature, atmospheric-pressure approaches have limited the application of such methods to Cu₂O-based devices. In particular, in the case of Cu₂O-based solar cells, the best results obtained so far have been achieved for high-temperature and vacuum-processing approaches and involving doping^{21,22}. Therefore, to harness the full potential of Cu₂O and other Cu-based materials, innovative low temperature and scalable deposition methods that are capable of yielding Cu₂O thin films with physical properties equivalent to those obtained with high-temperature and/or vacuum-based physical methods are needed.

In this context, atomic layer deposition (ALD) is gaining momentum in the last years due to its ability to offer good quality materials at low temperatures (<300 °C). In addition, the self-terminating, surface-limited reactions between gaseous precursors and the substrate surface allow depositing compact and continuous films with a subnanometer thickness control and unique conformality, even over high-aspect-ratio or complex/porous structures^{23,24}. These key assets have already been exploited in many laboratory-scale energy devices^{25–27}. But the vacuum processing and low deposition rate typically associated with ALD, limit its industrial application for low-cost energy devices. Atmospheric-pressure spatial atomic layer deposition (AP-SALD) is a recent approach that offers the same unique assets as ALD but at deposition rates comparable to chemical vapor deposition (CVD), and even working at atmospheric pressure. AP-SALD is compatible with roll-to-roll processing, and other in-line, fast atmospheric deposition techniques. Besides, the combination of AP-SALD and 3D printing technology in designing low-cost customized precursor injection heads allows the fabrication of

free-form motives without any pre patterning step²⁸. As a result of these unique assets, the main initial applications of AP-SALD were new generation solar cells and device encapsulation fields, in which low cost, scalability, and high deposition rate are critical features^{29,30}.

In ALD, the metal precursor has to fulfill simultaneously several critical requirements including high thermal stability, reactivity, good volatility, as well as cost-effectiveness. Several Cu ALD precursors have been used to date for the deposition of Cu₂O, such as Cu(hfac)₂^{31–33}, [Cu^{(5)Bu-Me-amd}]₂³⁴, [(hfac)Cu(I)(dmb)]₂³⁵, copper acetate (Cu(AcO)₂)³⁶, [Cu(tmhd)₂]³⁷, and Cu(dmap)₂^{38,39}. However, the growth per cycle (GPC) obtained in these studies is limited to a range of 0.004–0.012 nm/cycle, with a resulting low growth rate that varies from 0.001 to 0.003 nm/s. Adding to this, there are issues associated with the thermal decomposition of some of these Cu precursors^{31,36}. Interestingly, preliminary studies on the growth of Cu₂O thin films by AP-SALD showed one order of magnitude faster growth rates (0.016 nm/s) as compared with conventional ALD and promising results in terms of transport properties and application in ultralow-cost, all-oxide solar cells^{40,41}. Nevertheless, the properties of the films were still far from optimum due to the low thermal stability of the (hexafluoroacetylacetonate)-Cu(I)-(trimethylvinylsilane), Cu(hfac)(tmvs), a precursor used, which could represent a source of contamination in the obtained thin film⁴².

In this study, we report the open-air SALD growth of phase-pure Cu₂O thin films using a solid, stable precursor, namely copper(I) hexafluoro-2,4-pentanedionate cyclooctadiene complex, Cu(hfac)(cod), initially developed for CVD of metallic copper due to its high thermal stability and volatility^{43,44}. To the best of our knowledge, this is the first time that this precursor has been used to deposit Cu₂O by CVD, ALD, or SALD. Here, Cu₂O thin films have been deposited at low temperatures (<260 °C) with high deposition rates (0.018–0.059 nm/s). The morphological, optical, and transport properties have been studied. Remarkably, we have obtained high mobility values of up to $92 \text{ cm}^2 \text{ V}^{-1} \text{ s}^{-1}$, which are the result of a low concentration of shallow acceptor-like defects upon increasing the deposition temperature, as well as the limited role of the grain boundary scattering on the transport properties at room temperature. Optimized films have been used to fabricate submicron semitransparent solar harvesters based on Cu₂O/ZnO junctions.

Results and discussion

Deposition of Cu₂O thin films. Figure 1a shows a picture and the 3D chemical structure of the solid Cu(hfac)(cod) precursor (see Supplementary Table 1 for more details on the precursor). Given our SALD approach works in the open air (see Supplementary Fig. 1), a thermogravimetric analysis was performed to ensure proper evaporation and transport to the injection head while avoiding condensation in the lines or thermal decomposition. The results showed that there is a sensible weight loss already above 50 °C, while decomposition took place at around 145 °C (Supplementary Fig. 2). After optimization, the precursor temperature of 90 °C was chosen while the lines were heated at 95 °C to ensure that no condensation took place. Figure 1b shows two examples of homogeneous and semitransparent Cu₂O thin films deposited at 220 °C on borosilicate glass and a flexible substrate (Neopulim®—Transparent polyimide resin) with our home-built AP-SALD system. An XRD pattern of a 200-nm-thick Cu₂O film is shown in Fig. 1c. The (111) and (200) reflections of Cu₂O are clearly observed, without the presence of Cu or CuO reflections. The inset shows a SEM picture in which a continuous compact film can be observed. In general, ALD precursors must be volatile to ensure proper film deposition, and this is, even

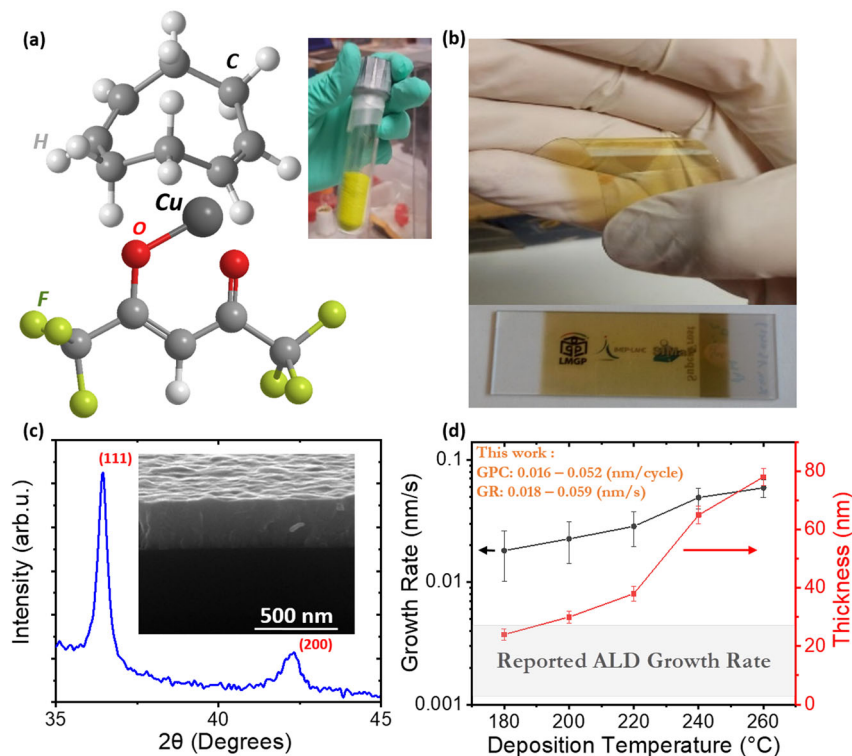


Fig. 1 Deposition of Cu_2O thin films using $\text{Cu}(\text{hfac})(\text{cod})$. **a** 3D scheme and picture (top right) of the $\text{Cu}(\text{hfac})(\text{cod})$ precursor used in this work. **b** Semitransparent Cu_2O thin films deposited on flexible Neopulim® (top) and borosilicate glass (bottom) substrates ($7.5 \text{ cm} \times 2.5 \text{ cm}$). **c** XRD pattern and SEM cross-section (inset) of a 200-nm-thick Cu_2O film deposited on a borosilicate glass substrate at $220 \text{ }^\circ\text{C}$ for 8000 cycles (160 min). **d** Growth rate and thickness variation of Cu_2O thin films deposited on glass at different temperatures (1500 cycles in all cases) along with the growth rate of conventional ALD as reported in the literature. Error bars represent the min/max values obtained for each point.

more, the case for systems working at atmospheric pressure, such as the AP-SALD one used here. In contrast, our report shows that solid precursors with relatively low volatility (0.1 mm Hg) can be used in atmospheric SALD systems to deposit intrinsic materials after proper optimization of the system and the deposition parameters. (While there have been two reports involving the use of a solid precursor in SALD, namely trimethylindium [$\text{In}(\text{CH}_3)_3$, (TLIn)], used to deposit $\text{In}_x\text{Ga}_y\text{Zn}_z\text{O}$ and $\text{In}_x\text{Zn}_{1-x}\text{O}$ ^{45,46} this precursor has a vapor pressure of 5 mm Hg , almost two orders of magnitude higher than the Cu precursor used here, and was used only to introduce doping).

The deposition was then carried out at different temperatures to evaluate the impact on the deposition rate and the physical properties of the obtained films (the deposition temperature was maintained below $260 \text{ }^\circ\text{C}$ in our study to prevent the formation of CuO ⁴⁰). Figure 1d shows the obtained thickness and growth rate as a function of deposition temperature (using 1500 cycles in all cases, which took 22 min). The obtained thickness varied from 24 to 78 nm (Supplementary Table 2), which corresponds to a GPC that increases from 0.016 nm/cycle at $180 \text{ }^\circ\text{C}$ to 0.052 nm/cycle at $260 \text{ }^\circ\text{C}$ (similar to previous results using $\text{Cu}(\text{hfac})(\text{tmvs})$ ⁴⁰). This corresponds to a growth rate that varies from 0.018 nm/s at $180 \text{ }^\circ\text{C}$ to 0.059 nm/s at $260 \text{ }^\circ\text{C}$, as shown in Fig. 1d. The reported GPC for other precursors used to deposit Cu_2O by ALD shows a GPC range varying from 0.006 to 0.012 nm/cycle , with the growth rate varying approximately from 0.001 nm/s to 0.003 nm/s ^{36,37,39}, the latter being about one order of magnitude lower than the maximum growth rate obtained in this work.

Chemical, structural, and optical characterization of Cu_2O thin films. The surface morphology of Cu_2O films prepared at 180 , 220 , and $260 \text{ }^\circ\text{C}$ was evaluated by SEM and AFM, as shown in

Fig. 2a, b. In all cases, both SEM and AFM results confirm the polycrystalline characteristic of deposited films with a larger mean grain size measured by both techniques for higher deposition temperatures (from roughly $30\text{--}70 \text{ nm}$, similar to our previous SALD report)⁴⁰. AFM measurements confirm the increase in grain size with temperature and show a slight roughness increase from 1.3 nm at $180 \text{ }^\circ\text{C}$ to 4.1 nm for the sample deposited at $260 \text{ }^\circ\text{C}$. But in all cases, RMS values below 4.1 nm are obtained. Figure 2c shows a TEM analysis of the cross-section of a 100-nm -thick cuprous oxide film deposited at $260 \text{ }^\circ\text{C}$. The image shows a columnar growth, as in previous SALD studies⁴⁰. This differs from other materials grown by SALD or other CVD methods, which show a pyramidal growth leading to increased grain size as the thickness of the film increases^{47,48}. Thus, the increase in the grain size is mainly attributed to the effect of deposition temperature on the grown thin films (see also Supplementary Fig. 3 for a comparison of films with the same thickness deposited at different temperatures). Selected-area electron diffraction, shown in Fig. 2c, confirms the crystallinity of the films, with diffraction rings matching the lattice spacing of Cu_2O and without other phases being detected. High-resolution TEM is also presented in Supplementary Fig. 4, where the crystallinity of the film is clearly observed.

The effect of deposition temperature on the composition, crystallinity, and texture of the films was also studied. Figure 3a shows the grazing incident (GI-XRD) patterns of films deposited at different temperatures, which in all cases show the (111) and (200) reflections of Cu_2O , with no Cu or CuO being detected. Despite the rather noisy signal shown in the Bragg-Brentano configuration due to the low thickness of the films ($\leq 78 \text{ nm}$ in all cases), as shown in Supplementary Fig. 5, a decrease in peak intensity of the (200) plane can be observed as temperature

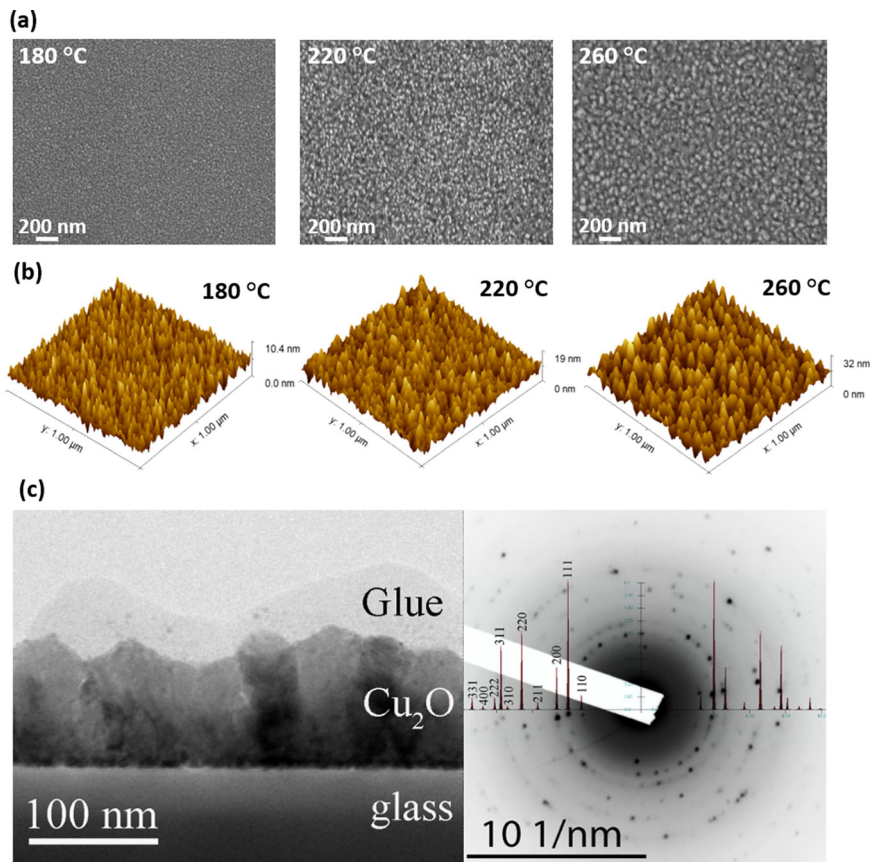


Fig. 2 Morphological characterization. **a** Secondary electron SEM pictures, **b** AFM topography images of Cu₂O thin films deposited on glass at different temperatures, and **c** Cross-section TEM analysis (left) and selected-area electron diffraction (SAED, right) of a Cu₂O film deposited at 260 °C for 2000 cycles. High-resolution TEM is shown in Supplementary Fig. 4.

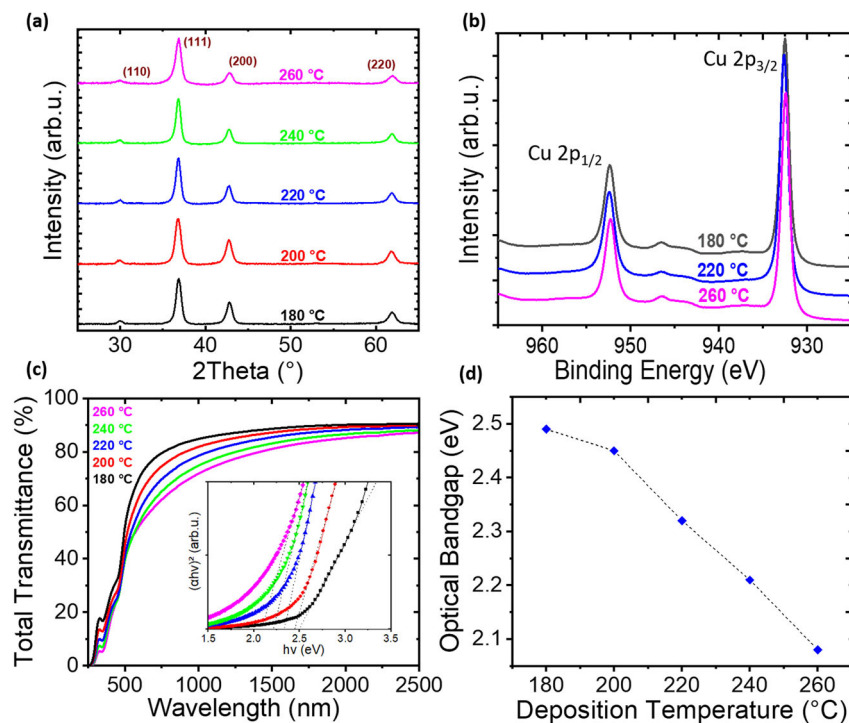


Fig. 3 Structural, chemical, and optical characterization. **a** GI-XRD patterns, **b** XPS spectra (Cu 2p region), **c** total transmittance and Tauc plot measurement (inset, extracted from transmittance and reflectance spectra), and **d** direct optical bandgap values of Cu₂O thin films deposited at different temperatures on borosilicate glass substrates. (Reflectance data are reported in Supplementary Fig. 9).

deposition increases, thus indicating a preferential growth orientation towards the (111) direction (also in agreement with the increase in roughness shown by AFM measurements⁴⁷). Therefore, an evolution of the texture of the films can be observed with temperature, going from patterns in which the (111) and (200) reflections have almost comparable intensities, towards a more preferential (111) orientation, comparable to the obtained for reference bulk samples. The calculated ratio between the (111) and (200) orientations for samples deposited at 180 °C and 260 °C tend to increase from (1:0.8) to (1:0.32), respectively. The following results are confirmed by the simulated modulus of the structure factor shown in Supplementary Fig. 6. Finally, a shift of the reflections to higher angles is also observed with increasing temperature, with respect to the ICDD reference pattern. This implies a slight decrease in cell parameters as the deposition temperature increased, which implies densification of the films, going from 5.81 g/cm³ at 180 °C to 5.9 g/cm³ at 260 °C (see Supplementary Fig. 6). This is in agreement with the obtained density of 5.86 ± 0.3 g/cm³ shown by X-ray reflectivity measurements of the sample deposited at 220 °C (Supplementary Fig. 7). Thus, the densities of the deposited films are very close to the density of single-crystal Cu₂O (6 g/cm³).

The chemical composition of the films and the oxidation state of Cu ions were further probed by XPS after 10 seconds of the Ar-etching process (Fig. 3b). The complete survey spectra can be found in Supplementary Fig. 8. The spectra show two peaks corresponding to the Cu 2p core levels at 932.2 eV and 951.1 eV, typical of Cu¹⁺. The satellite structure at approximately 943 eV typical of Cu²⁺ is not present in our spectra, thus ruling out partial oxidation of the films to CuO⁴⁹. Similarly, the spectra of the O 1s core level show a peak at 530.85 eV, which is typically observed for Cu¹⁺ in oxides (Supplementary Fig. 8).

The optical properties of the films were then characterized by UV-VIS spectroscopy. The total transmittance and reflectance were measured for the different films, having thicknesses that vary from 24 nm at 180 °C to 78 nm at 260 °C, to calculate the optical direct bandgap using the Tauc plot (as shown in Fig. 3c and Supplementary Fig. 9)⁵⁰. The absorption of the films in the UV region increases with deposition temperature, corresponding to a decrease of the optical bandgap of the layer from 2.5 to 2.08 eV (Fig. 3d). This is in agreement with previous studies that show such a decrease in the bandgap as the crystallinity and morphology of the material change^{51,52}. A wider bandgap in more amorphous phases is due to the short-range order present that displays an enlargement of the band edges into tails caused by the presence of localized energy states⁵³. The change of the optical bandgap in our films is also likely to be affected by the variation of the energy band structures induced by the change in the point defects.

Transport properties and Raman spectroscopy of Cu₂O thin films. The carrier concentration, mobility, and resistivity of the different films are presented in Fig. 4a. The films present a low resistivity in all cases, between 64 and 160 Ω.cm, comparable with the values obtained for Cu₂O thin films deposited by SALD with Cu(hfac)(tmvs) at similar temperatures⁴⁰. Notwithstanding, the results show that the hole carrier concentration tends to decrease from 2.10¹⁵ to 7.10¹⁴ cm⁻³ with increasing deposition temperature. Conversely, the mobility value obtained shows a clear increase from 42 to 92 cm²V⁻¹s⁻¹ for samples deposited from 200 to 260 °C, respectively. The mobility values obtained for the Cu₂O films deposited with Cu(hfac)(cod) are remarkably high, considering that the films are barely 40–70 nm in thickness and that they are deposited at low temperatures by a chemical approach. For instance, films deposited at 200 °C in this study

show mobility values that are one order of magnitude higher than for films deposited by AP-SALD using Cu(hfac)(tmvs) at similar temperatures (~4 cm²V⁻¹s⁻¹)⁴⁰. Even more remarkable, the mobility value obtained at 260 °C, above 90 cm²V⁻¹s⁻¹, is comparable to that of Cu₂O single crystals and epitaxial thin films⁵⁴. Figure 4b shows a graph in which the mobility of Cu₂O thin films deposited by different approaches vs. deposition temperature is presented. As it can be observed, the films deposited at 260 °C have the highest mobility values of all, while the films deposited between 200 and 240 °C have comparable mobility values than films deposited at 426 °C by DC-Sputtering⁵⁵, and are higher than for films deposited at 700 °C by RF-Sputtering⁵⁶. (A work by Akimoto et al. reporting the highest mobility value so far for Cu₂O films, i.e., 256 cm²V⁻¹s⁻¹, is not included in our comparison since in this study a buffer layer was used)⁵⁷.

To try to understand the high mobility values obtained here, the conductivity mechanism in Cu₂O needs to be evaluated. It is well known that the nature of p-type conductivity in Cu₂O is due to intrinsic defects, mainly copper vacancies and copper vacancies in the split configuration (where a copper atom is located halfway between a vacancy and an adjacent Cu position)^{14,15}. Normally, grain boundaries play a key role in the carrier mobility of semiconductors, especially for n-type, such as ZnO⁵⁸. In Cu₂O, the presence of CuO-rich regions in the grain boundaries has shown an effect on the conductivity of the films^{59,60}. Another study also points to the effect of the orientation on the conductivity of Cu₂O, which is impacted by the conductivity of interfaces⁶¹ (although the presence of CuO at the interfaces is not observed in this case). In a recent study by G. Aggarwal et al., it is shown that for single crystals and polycrystalline Cu₂O thin films, grain boundaries play a role in the mobility only at low temperatures but not at room temperature, where defects are the main parameter affecting mobility¹⁷. But it is worth noting that in this study, in all cases all the samples contain grains that are microns in size, and thus the number of grain boundaries is much lower than for typical CVD/ALD films that are made of nanometric crystals. Finally, the fact that films obtained from Cu(hfac)(tmvs) show similar particle sizes than films obtained from Cu(hfac)(cod)⁴⁰, while the mobility values of the former are much lower, confirms that mobility in Cu₂O is strongly affected by defects. The key parameter affecting the mobility at room temperature (both for polycrystalline films and single crystals) is indeed the trapping of holes by the acceptor-like intrinsic defects¹⁷. Therefore, the increase of the hole mobility with temperature shown in Fig. 4a, b could be explained by the decrease in the hole carrier concentration at higher deposition temperatures. This is also in agreement with the fact that films deposited from Cu(hfac)(tmvs) have one order of magnitude higher carrier concentration⁴⁰, which would explain their lower mobility as compared with films deposited at similar temperatures from Cu(hfac)(cod). A comparison of the Raman spectra of films deposited with the two precursors at the same temperature also shows that more defects are obtained when Cu(hfac)(tmvs) is used (see Supplementary Fig. 10 and discussion below).

To further probe the effect of defects on the mobility, the films obtained at different temperatures were analyzed by Raman spectroscopy. While Raman spectroscopy is mostly used to identify phases, it can also provide insights into the defects present. This is particularly the case for Cu₂O, which should present only one Raman active mode, but instead presents many peaks associated with the presence of intrinsic defects, regardless of the synthesis technique⁶². In particular, the T_{1u} (transversal and longitudinal) at 148, 624, and 649 nm and the second-order of an optical silent 2E_u mode at 235 nm are commonly observed (A 3D schematic representation of the Cu₂O vibrational modes giving rise to the different peaks can be found in Supplementary

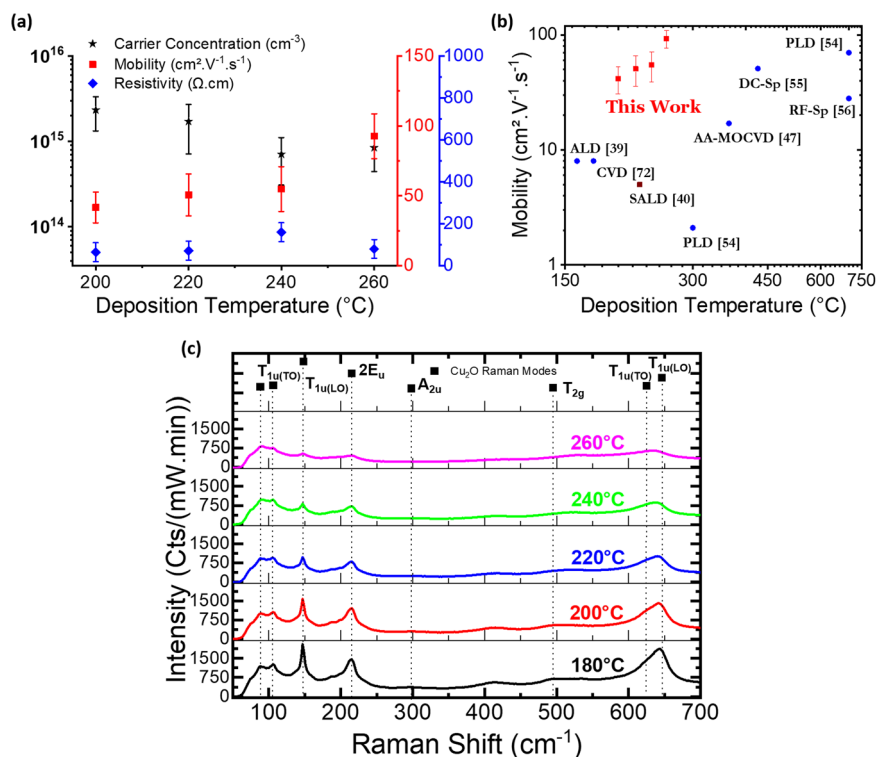


Fig. 4 Transport properties and Raman characterization. **a** Mobility, resistivity, and carrier concentration of Cu₂O thin films deposited at different deposition temperatures. **b** Mobility values for Cu₂O thin films obtained by different growth techniques as a function of deposition temperature (ALD³⁹, CVD⁷², SALD⁴⁰, PLD⁵⁴, AAMOCVD⁴⁷, DC-Sputtering⁵⁵, RF-Sputtering⁵⁶). **c** Raman spectra of Cu₂O thin films deposited on glass substrates at different deposition temperatures. Error bars represent the min/max values obtained for each point.

Fig. 11)⁶³. These extra peaks are the result of a perturbation of the material symmetry due to the presence of defects, in particular copper vacancies in the split configuration, as demonstrated by T. Sander et al.⁶². Figure 4c shows the Raman spectra of Cu₂O thin films deposited at different temperatures by SALD. In all cases, the expected peaks for Cu₂O are obtained, with no CuO being detected, in agreement with the XPS and TEM results shown above. But the intensity of the vibrational modes (T_{1u} and 2E_u) decreases with increasing deposition temperature. This result is counterintuitive since the films present a high crystallinity as the deposition temperature increases. Indeed, it implies that the amount of copper vacancies in the split configuration and probably normal copper vacancies decrease as the deposition temperature increases, which is again in agreement with the carrier concentration data obtained (Fig. 4a). In summary, as the deposition temperature increases, the concentration of copper vacancies in the split configuration decrease, which results in fewer trap centers and less charge scattering^{18,62,64}. As a result, and also thanks to the purity and high quality of the thin films deposited (i.e., high density), high mobility values have been obtained for non-epitaxial Cu₂O thin films deposited by chemical approaches at low temperature (Supplementary Fig. 12).

Given the excellent transport properties of the Cu₂O films deposited, a semitransparent solar harvester device combining extremely thin Cu₂O and ZnO layers, namely ~200 nm and ~130 nm (see SEM image in Fig. 5a), was fabricated and evaluated. The ZnO layer was also deposited by (AP-SALD) at 200 °C, as detailed in the experimental section. Figure 5b, c show a schematic view of the device structure (ITO)/ZnO/Cu₂O, and a picture of an actual, semitransparent, device with the Au top contacts deposited. Figure 5b shows a dark I-V curve (from -0.5 to +0.5 V) where a rectifying behavior is observed. The leakage current density was only 3×10^{-5} mA.cm⁻² at -0.5 V, while the current reached 0.9

mA.cm⁻² at +0.5 V. Under 1 sun illumination, the solar harvester exhibits a current density of 2 mA.cm⁻², a fill factor of 36%, and an open-circuit voltage of 0.111 V, which results in an efficiency of 0.26%, as shown in Fig. 5c. Figure 5d. shows the total transmittance, reflection, and absorbance of the device, showing that only wavelengths below 500 nm are efficiently harvested by the device, as expected for such a thin Cu₂O layer (see also Fig. 5e). The transparency in our device represents an important asset since it can be useful for implementation in building-integrated photovoltaic⁶⁹. In addition, the use of such thin films should allow better control over the mechanical properties and stress-induced to the bending of the device, especially for integrated devices⁷⁰.

The efficiency obtained is quite remarkable given the total thickness of the device and, in particular, the thickness of the ~200 nm thick Cu₂O absorber layer. Indeed, if compared with devices with similar thickness made by vacuum approaches, or with devices made by chemical approaches incorporating much thicker Cu₂O layers, the devices presented here are clearly superior. Figure 5f shows the performance obtained with ZnO/Cu₂O cells made by different approaches, including chemical deposition methods carried out at ambient pressure, both at low and high temperature. In all cases, the Cu₂O layer is one order of magnitude thicker than in our device, but the obtained J_{sc} and efficiency values are comparable (see Supplementary Table 3 for a comparison of the different cell parameters). This is also the case when comparing with a device having a similar thickness of Cu₂O, but in which both the ZnO and Cu₂O have been deposited by sputtering. If the current density and efficiency values are divided by the corresponding thickness of Cu₂O in each device, our device stands out as the one achieving a higher current density and efficiency per nanometer of absorber among all the devices. We ascribe the superior performances of our device to

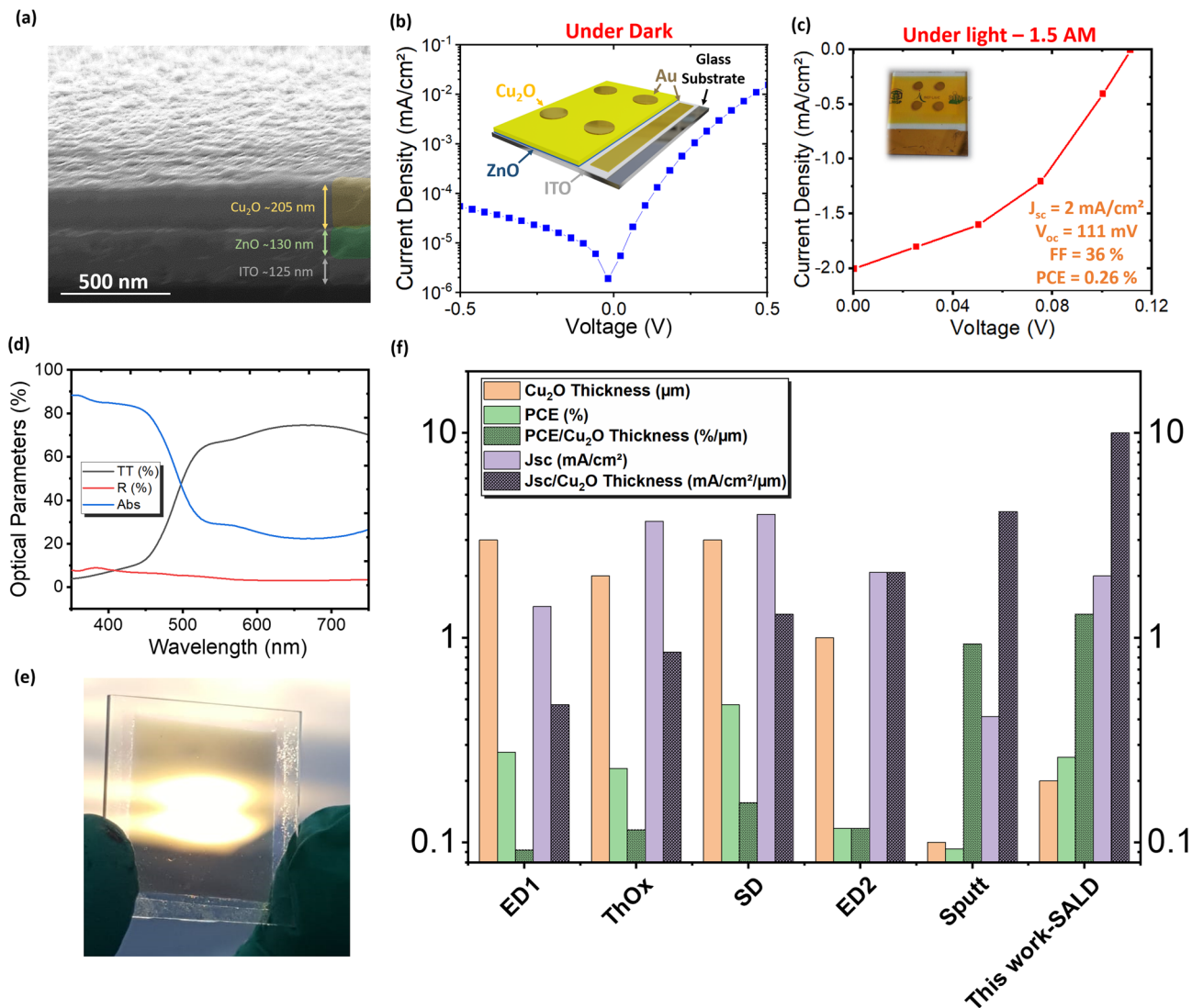


Fig. 5 Evaluation of $\text{Cu}_2\text{O}/\text{ZnO}$ devices. **a** SEM cross-section of a $\text{Cu}_2\text{O}/\text{ZnO}$ solar harvester. **b** Dark I-V curve of the fabricated $\text{Cu}_2\text{O}/\text{ZnO}$ PN heterojunction solar harvester (the inset shows a schematic view of the device). **c** Light I-V curve and resulting device parameters (the inset shows an image of the semitransparent solar harvester). **d** Total transmittance (TT), reflectance (R), and absorbance (Abs), of the $\text{Cu}_2\text{O}/\text{ZnO}$ solar harvester device deposited on top of an ITO/Glass substrate. **e** Image of the semitransparent device with a contrast of the sun illumination and the Néron mountain in the background. **f** Comparison between $\text{Cu}_2\text{O}/\text{ZnO}$ devices fabricated with different techniques (ED1⁶⁵-ThOx⁶⁶-SD⁶-ED2⁶⁷-Sputt⁶⁸). The following parameters are compared: Cu_2O thickness, power conversion efficiency (PCE), PCE/ Cu_2O thickness, current density " J_{sc} ", and $J_{sc}/\text{Cu}_2\text{O}$ thickness.

the good quality of the SALD Cu_2O layers obtained. (Indeed, the quality of the materials obtained by AP-SALD has already been exploited in new generation solar cells)^{29,71}.

Conclusion

In this study, a solid and stable Cu precursor, $\text{Cu}(\text{hfac})(\text{cod})$, has been used to deposit Cu_2O thin films by a CVD approach, namely, AP-SALD. The effect of the deposition temperature on the microstructure, optical, and transport properties of the obtained thin films has been studied. The films obtained are phase-pure and present good quality, with densities comparable to single-crystal Cu_2O . More remarkably, the films present in all cases show high mobility values, 1 order of magnitude higher than for Cu_2O thin films deposited previously by AP-SALD using $\text{Cu}(\text{hfac})(\text{tmvs})$, and even higher than the ones obtained for sputtered films deposited at much higher temperatures. A high mobility value of $92 \text{ cm}^2 \text{ V}^{-1} \text{ s}^{-1}$ has been obtained for the films deposited at 260°C , using a scalable, low temperature, and fast approach. Such high mobility values are explained by the

combination of low carrier concentration (in the range of 10^{14} – 10^{15} cm^{-3}) and the high quality of the films. In particular, Raman data shows a decrease in the number of copper vacancies in the split configuration as the deposition temperature increases, which can explain the enhanced mobility. Semitransparent $\text{Cu}_2\text{O}/\text{ZnO}$ solar harvesters have been fabricated using AP-SALD, showing high efficiency values when comparing to previous reports in which similar devices were fabricated using high-temperature and/or vacuum approaches, or in which much thicker Cu_2O layers were used. The reported results will surely provide relevant insights for further studies on Cu-based p-type semiconductors and, especially, for their application in photovoltaic and thin-film transistors.

Methods

Film deposition. Thin Cu_2O films were grown using a home-made SALD system equipped with a close-proximity manifold head (as described in our previous publications and schematized in Supplementary Fig. 1)⁴⁸. The films were deposited using Copper (I) Hexafluoro-2,4-Pentanedionate Cyclooctadiene ($\text{Cu}(\text{hfac})(\text{cod})$, from Epi-Valence Ltd.) and H_2O as a counter reactant. The precursor was heated at 90°C and the

transport line between the bubbler and the manifold injection head was heated at 95 °C to avoid any condensation of the precursors in the lines. Cu₂O films were deposited on borosilicate glass substrates with a surface area of 3 × 5 cm². The substrates were cleaned with isopropanol in an ultrasonic bath for 5 min and then dried with N₂. The substrate was maintained at a distance of 100 μm from the fixed injection head and oscillated at a speed of 10 cm/s. The precursor was delivered to the substrate by bubbling nitrogen (60 sccm) through the solid precursor, which was then diluted with an extra nitrogen flow (60 sccm) before being sent to the injection head. Further details related to the deposition process are described in Supplementary Note 1.

Characterization techniques. The surface morphology and thickness of Cu₂O thin films were characterized using a scanning electron microscopy (SEM-FEG) GeminiSEM 300 instrument. Film thickness was measured by ellipsometry (using a compact Film Sense FS-1 ellipsometer) and X-ray reflectometry (XRR, with a Siemens D500 model, using Cu K α radiation ($\lambda = 0.15406$ nm), 0.01°/step, 2 s/step). XRR data also provided information regarding the mass density, and surface roughness of the films. Atomic Force Microscopy (AFM) was used on the different layers in tapping mode using a Digital instrument D3100 Nanoscope. Transmission electron microscopy (TEM) imaging was performed with a JEOL JEM 2010 microscope operating at 200 kV model INCA Energy TEM 100 X-Max 65 T. X-ray Diffraction patterns were obtained with a Bruker D8 Advance diffractometer in the Bragg-Brentano (θ - 2θ) configuration, with Cu K α radiation (0.15406 nm). Grazing Incidence X-ray Diffraction (GI-XRD—Coplanar grazing incidence X-ray diffraction) acquisitions were collected on a RIGAKU Smartlab equipped with a 9 kW rotating anode Cu source (45 kV and 200 mA). Raman measurements were obtained in the wavenumber range of 50–700 cm⁻¹ using a Jobin Yvon/Horiba LabRam spectrometer equipped with a blue laser having a wavelength of 488 nm with a power of 0.8 mW for 10 min. The optical properties of the films were evaluated with a lambda 950 UV-Vis spectrophotometer from Perkin Elmer within the range of 250–2500 nm. The optical bandgaps of the different films were extracted from the transmittance and reflectance spectra using the Tauc plot method (Supplementary Fig. 9) and further details on the calculation method is given in SI^{18,50}. The electrical properties were measured with a Keithley 2400 source meter connected to a 4-point probe station in the Van der Pauw configuration at room temperature. A Hall Effect setup with a magnetic field of 0.5 Tesla was used to measure the carrier mobility and carrier concentration, for that the films were deposited on 1 × 1 cm² samples with evaporated gold contact on the top. X-ray photoelectron spectroscopy (XPS) spectra were obtained using a K-alpha spectrometer, from ThermoScientific, with an Al K α 1,2 (1486.6 eV) X-ray source. The samples were pretreated with an Ar-etching process at 2 KeV for 10 seconds. The thermal behavior of Cu(hfac)(cod) was evaluated with a thermogravimetric analyzer Setsys 16/18 Setaram analyzer with a heating range varying from 25 °C to 600 °C with a ramp of 10 °C/min and under argon atmosphere.

Device fabrication and testing. Cu₂O/ZnO solar cells were fabricated with the same approach (AP-SALD) on ITO/glass substrates from Delta Technologies. The thickness of ITO and glass substrate are 130 nm and 1.1 mm, respectively. The ITO/glass substrates were firstly cleaned with isopropanol and ethanol in an ultrasonic bath for 5 min each, and then dried with N₂. The deposition of the Cu₂O thin films was carried out at 220 °C for 2 h, resulting in a film thickness of about 200 nm. A ZnO layer was then deposited on the Cu₂O layer while the latter was maintained at 200 °C⁴⁸. Diethylzinc (C₂H₅)₂Zn (DEZ) from Sigma-Aldrich and H₂O were used as zinc and oxygen precursors (Further details related to the deposition process are described in Supplementary Note 1). Finally, gold electrodes (4 mm² surface area and 200 nm thick) were deposited using MEB550 E-beam evaporator from PLASYS on the top of the ZnO/Cu₂O/ITO/glass samples using a home-made metal mask (the same mask was used for the light I–V characterization). I–V curves were performed at room temperature with a Keithley 2400 source meter with a 2-tip probe station using a scan rate of 0.03 mA/s. For light I–V curves, a Newport solar simulator (model 67005) providing AM1.5 G illumination was used.

Reporting summary. Further information on research design is available in the Nature Research Reporting Summary linked to this article.

Data availability

The experimental raw data that support the findings of this study are available from the corresponding author upon reasonable request.

Received: 18 January 2021; Accepted: 30 June 2021;

Published online: 20 July 2021

References

- Grondahl, L. O. *Unidirectional Current Carrying Device*. US1640335A (1927). <https://worldwide.espacenet.com/patent/search/family/021694422/publication/US1640335A?q=pm%3DUS1640335A>
- IEA. *Global Energy and CO₂ Status Report*. *Oecd-Iea* 15 (IEA, 2018).
- Schmalensee, R. et al. *The Future of Solar Energy: An Interdisciplinary MIT Study* (Massachusetts Institute of Technology, 2015).
- Meyer, B. K. et al. Chapter six—the physics of copper oxide (Cu₂O). *Semicond. Semimetals* **88**, 201–226 (2013).
- Olsen, L. C., Addis, F. W. & Miller, W. Experimental and theoretical studies of Cu₂O solar cells. *Sol. Cells* **7**, 247–279 (1982).
- Musselman, K. P. et al. Strong efficiency improvements in ultra-low-cost inorganic nanowire solar cells. *Adv. Mater.* **22**, 254–258 (2010).
- Pan, L. et al. Cu₂O photocathodes with band-tail states assisted hole transport for stand-alone solar water splitting. *Nat. Commun.* **11**, 1–10 (2020).
- Paracchino, A., Laporte, V., Sivula, K., Grätzel, M. & Thimsen, E. Highly active oxide photocathode for photoelectrochemical water reduction. *Nat. Mater.* **10**, 456–461 (2011).
- Borgwardt, M. et al. Femtosecond time-resolved two-photon photoemission studies of ultrafast carrier relaxation in Cu₂O photoelectrodes. *Nat. Commun.* **10**, 1–7 (2019).
- Liu, A. et al. High-performance p-channel transistors with transparent Zn doped-CuI. *Nat. Commun.* **11**, 1–8 (2020).
- Steinhauer, S., Versteegh, M. A. M., Mysyrowicz, A., Kunert, B. & Zwiller, V. Cu₂O microcrystals grown on silicon as platform for quantum-degenerate excitons and rydberg states. *Commun. Mater.* **1**, 11 (2020).
- Jagt, R. A. et al. Rapid vapor-phase deposition of high-mobility p-type buffer layers on perovskite photovoltaics for efficient semitransparent devices. *ACS Energy Lett.* **5**, 2456–2465 (2020).
- Han, S. & Flewitt, A. J. Analysis of the conduction mechanism and copper vacancy density in p-type Cu₂O thin films. *Sci. Rep.* **7**, 1–8 (2017).
- Wright, A. F. & Nelson, J. S. Theory of the copper vacancy in cuprous oxide. *J. Appl. Phys.* **92**, 5849–5851 (2002).
- Raebiger, H., Lany, S. & Zunger, A. Origins of the p-type nature and cation deficiency in Cu₂O and related materials. *Phys. Rev. B Condens. Matter Mater. Phys.* **76**, 1–5 (2007).
- Scanlon, D. O., Morgan, B. J., Watson, G. W. & Walsh, A. Acceptor levels in p-type Cu₂O: rationalizing theory and Experiment. *Phys. Rev. Lett.* **103**, 1–4 (2009).
- Aggarwal, G., Maurya, S. K., Singh, A. J., Singh, A. K. & Kavaipatti, B. Intrinsic acceptor-like defects and their effect on carrier transport in polycrystalline Cu₂O photocathodes. *J. Phys. Chem. C* **123**, 26057–26064 (2019).
- Fleischer, K., Norton, E., Mullarkey, D., Caffrey, D. & Shvets, I. V. Quantifying the performance of P-type transparent conducting oxides by experimental methods. *Materials (Basel)* **10**, 19–22 (2017).
- Meyer, B. K. et al. Binary copper oxide semiconductors: from materials towards devices. *Phys. Status Solidi Basic Res.* **249**, 1487–1509 (2012).
- Fortin, E. & Weichman, F. L. Hall effect and electrical conductivity of Cu₂O monocrytals. *Can. J. Phys.* **44**, 1551–1561 (1966).
- Minami, T., Nishi, Y. & Miyata, T. Heterojunction solar cell with 6% efficiency based on an n-type aluminum-gallium-oxide thin film and p-type sodium-doped Cu₂O sheet. *Appl. Phys. Express* **8**, 022301 (2015).
- Lee, Y. S. et al. Atomic layer deposited gallium oxide buffer layer enables 1.2 V open-circuit voltage in cuprous oxide solar cells. *Adv. Mater.* **26**, 4704–4710 (2014).
- Meng, X. et al. Atomic layer deposition for nanomaterial synthesis and functionalization in energy technology. *Mater. Horizons* **4**, 133–154 (2017).
- Johnson, R. W., Hultqvist, A. & Bent, S. F. A brief review of atomic layer deposition: from fundamentals to applications. *Mater. Today* **17**, 236–246 (2014).
- Lu, H., Tian, W., Guo, J. & Li, L. Interface engineering through atomic layer deposition towards highly improved performance of dye-sensitized solar cells. *Sci. Rep.* **5**, 1–12 (2015).
- Bin, Mo, C. et al. Impact of buffer layer process and Na on shunt paths of monolithic series-connected CIGSSE thin film solar cells. *Sci. Rep.* **9**, 1–11 (2019).
- Ghobadi, A., Ghobadi, T. G. U., Karadas, F. & Ozbay, E. Angstrom thick ZnO passivation layer to improve the photoelectrochemical water splitting performance of a TiO₂ nanowire photoanode: the role of deposition temperature. *Sci. Rep.* **8**, 1–12 (2018).
- Arturo Masse de la Huerta, C. et al. Gas-phase 3D printing of functional materials. *Adv. Mater. Technol.* **5**, 2000657 (2020).
- Muñoz-Rojas, D. & Macmanus-Driscoll, J. Spatial atmospheric atomic layer deposition: a new laboratory and industrial tool for low-cost photovoltaics. *Mater. Horizons* **1**, 314–320 (2014).
- Muñoz-Rojas, D. et al. Dépôt spatial par couche atomique: un outil émergent pour les matériaux pour l'énergie. Application aux composants photovoltaïques de nouvelle génération et aux matériaux transparents et conducteurs. *Comptes Rendus Phys* **18**, 391–400 (2017).
- Zhong, Z., Wang, X., Ding, J. & Yuan, N. Nanometer-thick copper films grown by thermal atomic layer deposition. *Thin Solid Films* **589**, 673–680 (2015).

32. De Melo, C. et al. Local structure and point-defect-dependent area-selective atomic layer deposition approach for facile synthesis of p-Cu₂O/n-ZnO segmented nanojunctions. *ACS Appl. Mater. Interfaces* **10**, 37671–37678 (2018).
33. De Melo, C. et al. Semi-transparent p-Cu₂O/n-ZnO nanoscale-film heterojunctions for photodetection and photovoltaic applications. *ACS Appl. Nano Mater* **2**, 4358–4366 (2019).
34. Bae, H. et al. Solar-blind UV photodetector based on atomic layer-deposited Cu₂O and nanomembrane β -Ga₂O₃ pn oxide heterojunction. *ACS Omega* **4**, 20756–20761 (2019).
35. Kwon, J. D. et al. Controlled growth and properties of p-type cuprous oxide films by plasma-enhanced atomic layer deposition at low temperature. *Appl. Surf. Sci.* **285**, 373–379 (2013).
36. Iivonen, T. et al. Atomic layer deposition of photoconductive Cu₂O thin films. *ACS Omega* **4**, 11205–11214 (2019).
37. Dhakal, D. et al. Atomic layer deposition of ultrathin Cu₂O and subsequent reduction to Cu studied by in situ x-ray photoelectron spectroscopy. *J. Vac. Sci. Technol. A* **34**, 01A111 (2016).
38. Avila, J. R. et al. Atomic layer deposition of Cu(I) oxide films using Cu(II) bis(dimethylamino-2-propoxide) and water. *Dalt. Trans.* **46**, 5790–5795 (2017).
39. Kim, H. et al. Highly-conformal p-type copper(I) oxide (Cu₂O) thin films by atomic layer deposition using a fluorine-free amino-alkoxide precursor. *Appl. Surf. Sci.* **349**, 673–682 (2015).
40. Muñoz-Rojas, D. et al. Growth of ~ 5 cm²V⁻¹s⁻¹ mobility, p-type Copper(I) oxide (Cu₂O) films by fast atmospheric atomic layer deposition (AALD) at 225 °C and below. *AIP Adv.* **2**, 042179 (2012).
41. Marin, A. T. et al. Novel atmospheric growth technique to improve both light absorption and charge collection in ZnO/Cu₂O thin film solar cells. *Adv. Funct. Mater.* **23**, 3413–3419 (2013).
42. Pirolli, L. & Teplyakov, A. V. Adsorption and thermal chemistry of 1,1,1,5,5,5-hexafluoro-2,4-pentanedione (hfach) and (hexafluoroacetylacetonate)Cu(vinyltrimethylsilane) ((hfac)Cu(VTMS)) on TiCN-covered Si(1 0 0) surface. *Surf. Sci.* **601**, 155–164 (2007).
43. Chi, K. M., Shin, H. K., Hampden-Smith, M. J., Duesler, E. N. & Kodas, T. T. The chemistry of β -diketonate copper(I) compounds-III. The synthesis of (β -diketonate) Cu(1,5-COD) compounds, the solid state structure and disproportionation of hexafluoroacetylacetonato (1,5-cyclooctadiene)copper (I), (hfac)Cu(1,5-COD). *Polyhedron* **10**, 2293–2299 (1991).
44. Shin, H. K., Hampden-Smith, M. J., Kodas, T. T. & Rheingold, A. L. Synthesis of volatile, fluorinated β -ketoiminato copper(I) complexes. *J. Chem. Soc. Chem. Commun.* 217–219 (1992).
45. Illiberi, A. et al. Spatial atmospheric atomic layer deposition of In₂Ga₂Zn₂O for thin film transistors. *ACS Appl. Mater. Interfaces* **7**, 3671–3675 (2015).
46. Illiberi, A. et al. Atmospheric plasma-enhanced spatial-ALD of InZnO for high mobility thin film transistors. *J. Vac. Sci. Technol. A* **36**, 04F401 (2018).
47. Liu, H. et al. The role of humidity in tuning the texture and electrical properties of Cu₂O thin films deposited via aerosol-assisted CVD. *Adv. Mater. Interfaces* **6**, 1–10 (2019).
48. Nguyen, V. H. et al. Deposition of ZnO based thin films by atmospheric pressure spatial atomic layer deposition for application in solar cells. *J. Renew. Sustain. Energy* **9**, 021203 (2017).
49. Li, J. et al. Probing defects in nitrogen-doped Cu₂O. *Sci. Rep.* **4**, 1–6 (2014).
50. Tauc, J. & Menth, A. States in the gap. *J. Non. Cryst. Solids* **8–10**, 569–585 (1972).
51. Zanatta, A. & Chambouleyron, I. Absorption edge, band tails, and disorder of amorphous semiconductors. *Phys. Rev. B Condens. Matter Mater. Phys* **53**, 3833–3836 (1996).
52. Anderson, P. W. Absence of diffusion in certain random lattices. *Phys. Rev.* **109**, 1492–1505 (1958).
53. Biederman, H. *Plasma Polymer Films* (Imperial College Press, 2004).
54. Matsuzaki, K. et al. Epitaxial growth of high mobility Cu₂O thin films and application to p-channel thin film transistor. *Appl. Phys. Lett.* **93**, 3–6 (2008).
55. Murali, D. S. et al. Synthesis of Cu₂O from CuO thin films: optical and electrical properties. *AIP Adv.* **5**, 1–6 (2015).
56. Han, S., Niang, K. M., Rughoobur, G. & Flewitt, A. J. Effects of post-deposition vacuum annealing on film characteristics of p-type Cu₂O and its impact on thin film transistor characteristics. *Appl. Phys. Lett.* **109**, 173502 (2016).
57. Li, B. S., Akimoto, K. & Shen, A. Growth of Cu₂O thin films with high hole mobility by introducing a low-temperature buffer layer. *J. Cryst. Growth* **311**, 1102–1105 (2009).
58. Nguyen, V. H. et al. Electron tunneling through grain boundaries in transparent conductive oxides and implications for electrical conductivity: The case of ZnO:Al thin films. *Mater. Horizons* **5**, 715–726 (2018).
59. Deuermeier, J. et al. Visualization of nanocrystalline CuO in the grain boundaries of Cu₂O thin films and effect on band bending and film resistivity. *APL Mater.* **6**, 096103 (2018).
60. Deuermeier, J. et al. Highly conductive grain boundaries in copper oxide thin films. *J. Appl. Phys.* **119**, 235303 (2016).
61. Tibério, M. et al. Orientation dependence of electrical properties of polycrystalline Cu₂O thin films. *Semicond. Sci. Technol.* **35**, 075016 (2020).
62. Sander, T. et al. Correlation of intrinsic point defects and the Raman modes of cuprous oxide. *Phys. Rev. B Condens. Matter Mater. Phys* **90**, 1–8 (2014).
63. Sander, T. *Monitoring defect-induced perturbations of the ideal crystal structure of ZnO and Cu₂O by Raman spectroscopy* (I. Physikalisches Institut Justus-Liebig-Universität Gießen, 2015).
64. Hautier, G., Miglio, A., Ceder, G., Rignanese, G. M. & Gonze, X. Identification and design principles of low hole effective mass p-type transparent conducting oxides. *Nat. Commun.* **4**, 1–7 (2013).
65. Jeong, S. S., Mittiga, A., Salza, E., Masci, A. & Passerini, S. Electrodeposited ZnO/Cu₂O heterojunction solar cells. *Electrochim. Acta* **53**, 2226–2231 (2008).
66. Ievskaya, Y., Hoye, R. L. Z., Sadhanala, A., Musselman, K. P. & MacManus-Driscoll, J. L. Fabrication of ZnO/Cu₂O heterojunctions in atmospheric conditions: Improved interface quality and solar cell performance. *Sol. Energy Mater. Sol. Cells* **135**, 43–48 (2015).
67. Katayama, J., Ito, K., Matsuoka, M. & Tamaki, J. Performance of Cu₂O/ZnO solar cell prepared by two-step electrodeposition. *J. Appl. Electrochem.* **34**, 687–692 (2004).
68. Rana, A. K., Park, J. T., Kim, J. & Wong, C. P. See-through metal oxide frameworks for transparent photovoltaics and broadband photodetectors. *Nano Energy* **64**, 103952 (2019).
69. Ballif, C., Perret-Aebi, L. E., Lufkin, S. & Rey, E. Integrated thinking for photovoltaics in buildings. *Nat. Energy* **3**, 438–442 (2018).
70. Zhu, R., Zhang, Z. & Li, Y. Advanced materials for flexible solar cell applications. *Nanotechnol. Rev.* **8**, 452–458 (2019).
71. Raninga, R. D. et al. Strong performance enhancement in lead-halide perovskite solar cells through rapid, atmospheric deposition of n-type buffer layer oxides. *Nano Energy* **75**, 104946 (2020).
72. Eisermann, S. et al. Copper oxide thin films by chemical vapor deposition: Synthesis, characterization and electrical properties. *Phys. Status Solidi Appl. Mater. Sci.* **209**, 531–536 (2012).

Acknowledgements

This work has been partially supported by the CDP Eco-SESA receiving funds from the French National Research Agency in the framework of the “Investments for the future” program (ANR-15-IDEX-02). D.M.R. acknowledges support from the European Union’s Horizon 2020 FETOPEN-1-2016-2017 research and innovation program under Grant Agreement 801464, and through the Marie Curie Actions (FP7/2007-2013, Grant Agreement No. 63111). We thank the Agence Nationale de la Recherche (ANR, France) via the projects DESPATCH (No. ANR-16-CE05-0021) and OXYGENE (ANR-17-CE05-0034) and Carnot energies du future. We would like to warmly thank Maciej Oskar Liedke, Thomas Sander, Odette Chaix, Hervé Roussel, and Simon Rushworth for fruitful discussions.

Author contributions

A.S., V.H.N., and C.A.M.H. performed experiments. L.R. performed TEM characterization and analysis. Experimental data was analyzed under the supervision of A.K.C., G.C., D.B., and D.M.R. All authors contributed to the interpretation of the results. A.S. and D.M.R. wrote the manuscript.

Competing interests

The authors declare no competing interests.

Additional information

Supplementary information The online version contains supplementary material available at <https://doi.org/10.1038/s43246-021-00181-8>.

Correspondence and requests for materials should be addressed to D.Mñio-R.

Peer review information *Communications Materials* thanks the anonymous reviewers for their contribution to the peer review of this work. Primary Handling Editors: Cecilia Mattevi and Aldo Isidori.

Reprints and permission information is available at <http://www.nature.com/reprints>

Publisher’s note Springer Nature remains neutral with regard to jurisdictional claims in published maps and institutional affiliations.



Open Access This article is licensed under a Creative Commons Attribution 4.0 International License, which permits use, sharing, adaptation, distribution and reproduction in any medium or format, as long as you give appropriate credit to the original author(s) and the source, provide a link to the Creative Commons license, and indicate if changes were made. The images or other third party material in this article are included in the article's Creative Commons license, unless indicated otherwise in a credit line to the material. If material is not included in the article's Creative Commons license and your intended use is not permitted by statutory regulation or exceeds the permitted use, you will need to obtain permission directly from the copyright holder. To view a copy of this license, visit <http://creativecommons.org/licenses/by/4.0/>.

© The Author(s) 2021